chemosensors

MDPI

Article

High Sensitivity Low-Temperature Hydrogen Sensors Based on SnO_2/κ(ε)-Ga_2O_3:Sn Heterostructure

Aleksei Almaev [1,2,*], Nikita Yakovlev [1], Viktor Kopyev [1], Vladimir Nikolaev [3,4], Pavel Butenko [3], Jinxiang Deng [5], Aleksei Pechnikov [3], Petr Korusenko [6,7], Aleksandra Koroleva [8] and Evgeniy Zhizhin [8]

1 Research and Development Centre for Advanced Technologies in Microelectronics, National Research Tomsk State University, 634050 Tomsk, Russia; nik_mr_x@mail.ru (N.Y.); viktor.kopev@gmail.com (V.K.)
2 Fokon Limited Liability Company, 248035 Kaluga, Russia
3 Ioffe Institute of the Russian Academy of Sciences, 194021 Saint Petersburg, Russia; pavel.butenko@mail.ioffe.ru (P.B.); alpechn@yandex.ru (A.P.)
4 Perfect Crystals Limited Liability Company, 194223 Saint Petersburg, Russia
5 Department of Condensed Matter Physics, Faculty of Science, Beijing University of Technology, Beijing 100124, China; jdeng@bjut.edu.cn
6 Department of Solid State Electronics, Saint Petersburg State University, 199034 Saint Petersburg, Russia; korusenko_petr@mail.ru
7 Department of Physics, Omsk State Technical University, 644050 Omsk, Russia
8 Research Park, Saint Petersburg State University, 199034 Saint Petersburg, Russia; koroleva.alexandra.22@gmail.com (A.K.); evgeny_liquid@mail.ru (E.Z.)
* Correspondence: almaev_alex@mail.ru

Abstract: The structural and gas-sensitive properties of *n-N* SnO_2/κ(ε)-Ga_2O_3:Sn heterostructures were investigated in detail for the first time. The κ(ε)-Ga_2O_3:Sn and SnO_2 films were grown by the halide vapor phase epitaxy and the high-frequency magnetron sputtering, respectively. The gas sensor response and speed of operation of the structures under H_2 exposure exceeded the corresponding values of single κ(ε)-Ga_2O_3:Sn and SnO_2 films within the temperature range of 25–175 °C. Meanwhile, the investigated heterostructures demonstrated a low response to CO, NH_3, and CH_4 gases and a high response to NO_2, even at low concentrations of 100 ppm. The current responses of the SnO_2/κ(ε)-Ga_2O_3:Sn structure to 10^4 ppm of H_2 and 100 ppm of NO_2 were 30–47 arb. un. and 3.7 arb. un., correspondingly, at a temperature of 125 °C. The increase in the sensitivity of heterostructures at low temperatures is explained by a rise of the electron concentration and a change of a microrelief of the SnO_2 film surface when depositing on κ(ε)-Ga_2O_3:Sn. The SnO_2/κ(ε)-Ga_2O_3:Sn heterostructures, having high gas sensitivity over a wide operating temperature range, can find application in various fields.

Keywords: κ(ε)-Ga_2O_3:Sn; SnO_2; HVPE; magnetron sputtering; *n-N* heterostructure; gas sensors

Citation: Almaev, A.; Yakovlev, N.; Kopyev, V.; Nikolaev, V.; Butenko, P.; Deng, J.; Pechnikov, A.; Korusenko, P.; Koroleva, A.; Zhizhin, E. High Sensitivity Low-Temperature Hydrogen Sensors Based on SnO_2/κ(ε)-Ga_2O_3:Sn Heterostructure. *Chemosensors* **2023**, *11*, 325. https://doi.org/10.3390/chemosensors11060325

Academic Editor: Elisabetta Comini

Received: 17 April 2023
Revised: 24 May 2023
Accepted: 29 May 2023
Published: 1 June 2023

1. Introduction

Sustainable development in terms of preserving the environment requires employment of a great number of sensors: biosensors, image sensors, motion sensors, and chemical sensors for indoor and outdoor as well as for industry-relevant gas surveillance and control. Wide bandgap metal oxide semiconductors tin dioxide (SnO_2) and gallium oxide (Ga_2O_3) are of high interest for the development of gas sensors and transparent contacts, finding applications in a number of devices [1–6]. Heterostructures based on metal oxide semiconductors allow the advantages of each component to be combined in a single structure [7]. Thus, superior gas-sensitive characteristics can be achieved for heterostructures compared to single semiconductors. It is reasonable to combine semiconductors with high catalytic activity and concentration of electrons, involved in the physico–chemical processes at chemisorption of gas molecules on the semiconductor surface.

SnO_2 is one of the most studied metal oxide semiconductors for gas sensor applications [1] primarily due to its high catalytic activity, which leads to a high gas sensitivity compared to other metal oxides. Chemisorption of gas molecules on the SnO_2 surface occurs with the involvement of free electrons. However, pure SnO_2 does not have a high electron concentration. Localization of electrons in this semiconductor can be achieved by forming heterostructures. Ga_2O_3 with an electron affinity χ = 4.0 eV can be paired with SnO_2, which is characterized by χ = 5.32 eV [8], to form such a heterostructure. In turn, Ga_2O_3 needs to be doped to achieve the required concentration of free electrons. In this case, one can expect an increase in the sensitivity of such heterostructure to gases as compared to pure SnO_2 and Ga_2O_3 films.

Gallium oxide has several polymorphs [9–12] namely α, β, γ, δ, and κ(ε). Metastable κ(ε)-Ga_2O_3 polymorph is of particular interest for the development of electronic devices due to its fundamental properties [13] such as the thermal stability up to 700 °C; the high bandgap E_g of 4.5–5.0 eV; availability of the ferroelectric properties; the high symmetry of a crystal lattice. κ(ε)-Ga_2O_3 is a novel material in terms of sensors, since its gas sensitivity was researched for the first time in 2022 [14]. We have demonstrated that κ(ε)-Ga_2O_3:Sn films grown by the halide vapor phase epitaxy (HVPE) have a low resistance (i.e., high electron concentration), stable characteristics in the temperature range from 20 °C to 500 °C, and exhibit sensitivity to H_2 at room temperature (*RT*) [14]. In addition, the κ(ε)-Ga_2O_3 polymorph meets the conditions of heteroepitaxy on a commercially available (0001) Al_2O_3 substrate better than monoclinic β-Ga_2O_3 [15]. Thus, doped κ(ε)-Ga_2O_3:Sn can be chosen to pair with SnO_2 to form a heterostructure.

SnO_2/β-Ga_2O_3 and SnO_2/κ(ε)-Ga_2O_3 heterostructures have previously been investigated for the development of power diodes [16,17] and solar-blind avalanche photodetectors with high sensitivity [8]. β-Ga_2O_3 nanostructures covered with ultrathin layers of SnO_2 demonstrated high sensitivity to ethanol at T = 400 °C [18] and to H_2 in the range of T = 25–200 °C [19]. The gas-sensitive properties of SnO_2/κ(ε)-Ga_2O_3:Sn heterostructures have not been studied before.

The purpose of this work is to gain insight into the gas-sensitive properties of SnO_2/κ(ε)-Ga_2O_3:Sn heterostructures.

2. Materials and Methods

The following films were deposited on (0001) single crystal Al_2O_3 substrates: κ(ε)-Ga_2O_3:Sn and SnO_2 thin films as well as SnO_2/κ(ε)-Ga_2O_3:Sn heterostructure. The process of the κ(ε)-Ga_2O_3:Sn films growth was multistage. In the first stage, a 3-µm-thick semi-insulating (SI) GaN layer was deposited on the Al_2O_3 substrate by gas phase deposition employing a homemade reactor. This layer served as a template for the κ(ε)-Ga_2O_3:Sn film growth. In the second stage, a 1-µm-thick κ(ε)-Ga_2O_3 layer in situ doped by Sn was deposited on the SI-GaN layer by HVPE using a hot-wall homemade reactor. Gaseous gallium chloride and oxygen were utilized as precursors. The doping of the κ(ε)-Ga_2O_3 films was carried out during the growth by adding tin. The HVPE growth temperature of the κ(ε)-Ga_2O_3:Sn film was 600 °C. The analysis of current–voltage (*I*–*V*) and capacitance–voltage (*C*–*V*) characteristics applied at this stage showed that the effective donor concentration N_d of the films was 5.13 × 10^{20} cm^{-3}.

120-nm-thick pure SnO_2 thin films were deposited by means of magnetron sputtering of an Sn (5N) target in an oxygen–argon plasma on Al_2O_3 and κ(ε)-Ga_2O_3:Sn. An Edwards A-500 (Edwards, USA) setup was employed. To prepare SnO_2/κ(ε)-Ga_2O_3:Sn heterostructures, SnO_2 thin films were deposited through a mask with square-shaped slots of 1 mm × 1 mm. The temperature of substrates during the deposition of the film was *RT*. The working pressure and power were kept at 7 × 10^{-3} mbar and 70 W, respectively. The oxygen concentration in the O_2+Ar mixture was 56.1 ± 0.5 vol. %. The as-deposited SnO_2 films were annealed ex situ at T = 600 °C; for 4 hours in air. The estimates showed that the N_d value of these films was 5.26 × 10^{17} cm^{-3}.

Pt contacts were deposited on the κ(ε)-Ga_2O_3:Sn and SnO_2 films (see Figure 1) by means of the magnetron sputtering. Pt contacts were chosen on the basis of their high stability at high temperatures and under exposure to various gases, which are of natural surroundings- and industrial relevance.

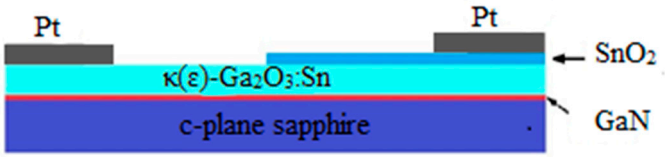

Figure 1. Schematic of the SnO_2/κ(ε)-Ga_2O_3:Sn heterostructure.

X-ray diffraction (XRD) analysis of the samples was performed at DRON-6 diffractometer (Bourevestnik, Petersburg, Russia) equipped with a copper anode ($CuK_{\alpha 1}$, λ = 1.5406 Å). The XRD patterns were registered in θ-2θ scanning mode. The phase composition of the samples was identified by the position of the reflection peaks. XRD θ-2θ curves were processed using the Scherrer method [20] to determine the characteristic size of the block in the direction perpendicular to the plane of epitaxial growth.

The chemical composition of the samples was studied by X-ray photoelectron spectroscopy (XPS). The XPS measurements were carried out using a hemispherical analyzer included in the ESCALAB 250Xi (Thermo Fisher Scientific, Waltham, MA, USA) laboratory spectrometer. The measurements were carried out using a monochromatized AlK_a radiation ($h\nu$ = 1486.6 eV). Survey and core (O1s, Sn3d, Ga3d) photoemission (PE) spectra were recorded at the analyzer transmission energy of 100 and 50 eV, respectively. The film's surface was irradiated with argon ions at an average energy of 3 eV for 60 s before XPS measurements to remove adsorbed atoms and molecules of contaminants. The analysis of the core spectra was processed employing the Avantage Data System software.

Measurement of transmission spectra was carried out using an Ocean Optics (Ocean Insight, Orlando, FL, USA) spectrometric system to determine the E_g of SnO_2 in the wavelength range of λ = 300–600 nm. The transmission spectrum of κ(ε)-Ga_2O_3:Sn films was measured using a UV-VIS two-beam SPECORD (Analytik Jena, Jena, Germany) spectrophotometer in the range of λ = 230–360 nm.

A high-resolution field emission scanning electron microscope (FESEM) Apreo 2S (Thermo Fisher Scientific, USA) operating at an accelerating voltage of 5 kV was employed to study the microrelief of the film surfaces with a high resolution.

Gas sensing measurements of the samples were performed in a dedicated sealed chamber with a volume of 100 cm^3, equipped with a micro-probe Nextron MPS-CHH station (Nextron, Busan, Republic of Korea). A ceramic-type heater, installed in the sealed chamber, was used to heat the samples. The accuracy of temperature T control was ±0.1 °C. The experiments were carried out under dark conditions. Streams of pure dry air or gas mixture of pure dry air + H_2 were pumped through the chamber to measure the gas sensing characteristics of the samples. The H_2 concentration in the mixture was controlled by a gas mixing and delivery system Microgas F-06 (Intera, Moscow, Russia). A special generator (Khimelektonika SPE, Moscow, Russia) was used to produce pure dry air. The total flow rate of the gas mixtures through the chamber was 1000 sccm. The relative error of the gas mixture flow rate did not exceed 1.5%. A Keithley 2636 A (Keithley, Solon, OH, USA) source meter was utilized to measure the time dependences of the current I and the I–V characteristics of the samples. An E4980A RLC-meter (Agilent, Santa Clara, CA, USA) was applied to measure the C–V dependences. Additionally, gas sensing measurements of the samples were carried out under exposure to NH_3, CH_4, CO, NO_2, and O_2. A mixture of N_2 + O_2 was used to study the sensitivity of samples to O_2. To study the effect of relative humidity (RH) on the response of the samples to H_2, the pure dry air in one of the channels was passed through a bubbler with distilled water. Then it entered the homogenizer, where it was mixed with the pure dry air and/or pure dry air + H_2 mixture streams from the other channels. Varying the ratio of flows through the channels, we set the desired level of RH in

the measuring chamber. An HIH 4000 Honeywell capacitive sensor with an absolute error of ±3.5% was used to measure the *RH*. Just prior to these measurements, all the samples were subjected to heat treatment at T = 500 °C for 90 s in pure dry air to stabilize the contact properties and regenerate the surface.

3. Results and Discussion

3.1. Structural Properties

Figure 2a illustrates the θ-2θ XRD pattern of the SnO_2/Ga_2O_3 heterostructure deposited on an Al_2O_3 substrate via a GaN template. The peaks at 2θ = 41.8° and 90.9° are associated with the (0006) and (0 0 0 12) reflections of the Al_2O_3 substrate (ICDD # 00-042-1468). A series of peaks at 2θ = 19.2°, 39.0°, 60.0°, 83.6°, and 112.7° correspond to the 002, 004, 006, 008, and 0 0 10 planes of the κ(ε)-Ga_2O_3 phase. (The calculation was made on the basis of the Bragg equation for the case of $CuK_{\alpha 1}$ anode (λ = 1.5406 Å). The peaks at 2θ = 34.7°, 73.0°, and 126.1° are due to the (0002), (0004), and (0006) reflections of the GaN template (AMCSD # 99-101-0461). Peaks corresponding to SnO_2 could not be distinguished due to possible overlapping by neighboring reflections of other phases. Thus, the (101) reflection of SnO_2 (AMCSD no. 99-100-8661) is close to the (0002) one of GaN, and the (111) reflection of SnO_2 is close to the (004) one of κ(ε)-Ga_2O_3. The auxiliary vertical red lines of equal intensity depicted in Figure 2a are the tabular values of the SnO_2 reflection positions. In addition, difficulties in SnO_2 peaks identification may be caused by the low film thickness and the developed microrelief of the surface. Finally, the possible low crystallinity of the SnO_2 phase may be the reason for the absence of sharp peaks on the XRD pattern. In this case, broad humps of a low intensity may be present.

κ(ε)-Ga_2O_3:Sn and SnO_2 films are characterized by direct optical transitions according to the analysis of transmission spectra (see Figure 2b), where α is the absorption coefficient. E_g values were graphically calculated and proved to be equal to 4.61 ± 0.01 eV and 3.76 ± 0.01 eV for the κ(ε)-Ga_2O_3:Sn and SnO_2 films, respectively.

According to XPS analysis, the composition of the SnO_2 film includes Sn and O elements only. However, carbon (C) as a common contaminant was also observed in the subsurface layer a few nanometers thick. C atoms completely disappear after argon-etching for 60 s. Ga, Sn, O, and C lines were observed in the survey PE spectra of κ(ε)-Ga_2O_3:Sn film. The Sn concentration in this film appeared to be about 3 at. %, which indicates a high level of doping. Thus, the chemical analysis has shown that there are no third-party impurities in the composition of κ(ε)-Ga_2O_3:Sn and SnO_2 films, which confirms the high purity of the deposited films.

The analysis of the chemical state of Sn based on the $Sn3d_{5/2}$ PE line revealed the energy position of the main maximum of Sn at 486.5 and 486.3 eV (Figure 2c). The obtained values are in good agreement with the literature data [21,22] and correspond to the higher oxidation state of Sn–SnO_2 oxide. A lower value of the SnO_2 energy position for the κ(ε)-Ga_2O_3:Sn film indicates the effect of Ga_2O_3 on the charge state of SnO_2. Previously, we have observed a similar effect of the $Sn3d_{5/2}$ PE line shift to low binding energies of the SnO_2 film doped with rare-earth elements and platinum group metals [21,22]. Analysis of the Ga chemical state in the κ(ε)-Ga_2O_3:Sn film based on the Ga3d PE line showed that Ga corresponds to the higher Ga_2O_3 oxide [23] (Figure 2d).

FESEM images of the SnO_2 films surface deposited on Al_2O_3 substrates and κ(ε)-Ga_2O_3:Sn film are displayed in Figure 2e,f, respectively. The microrelief of the SnO_2 film on Al_2O_3 (Figure 2e) contains small spherical grains with a diameter of ~35 nm and large agglomerates with a characteristic size of ~300 nm. Whereas the microrelief of the SnO_2 film deposited on a κ(ε)-Ga_2O_3:Sn one (see Figure 2f) is represented by small grains with a diameter of ~35 nm only. The formation of large agglomerates for these structures was not observed.

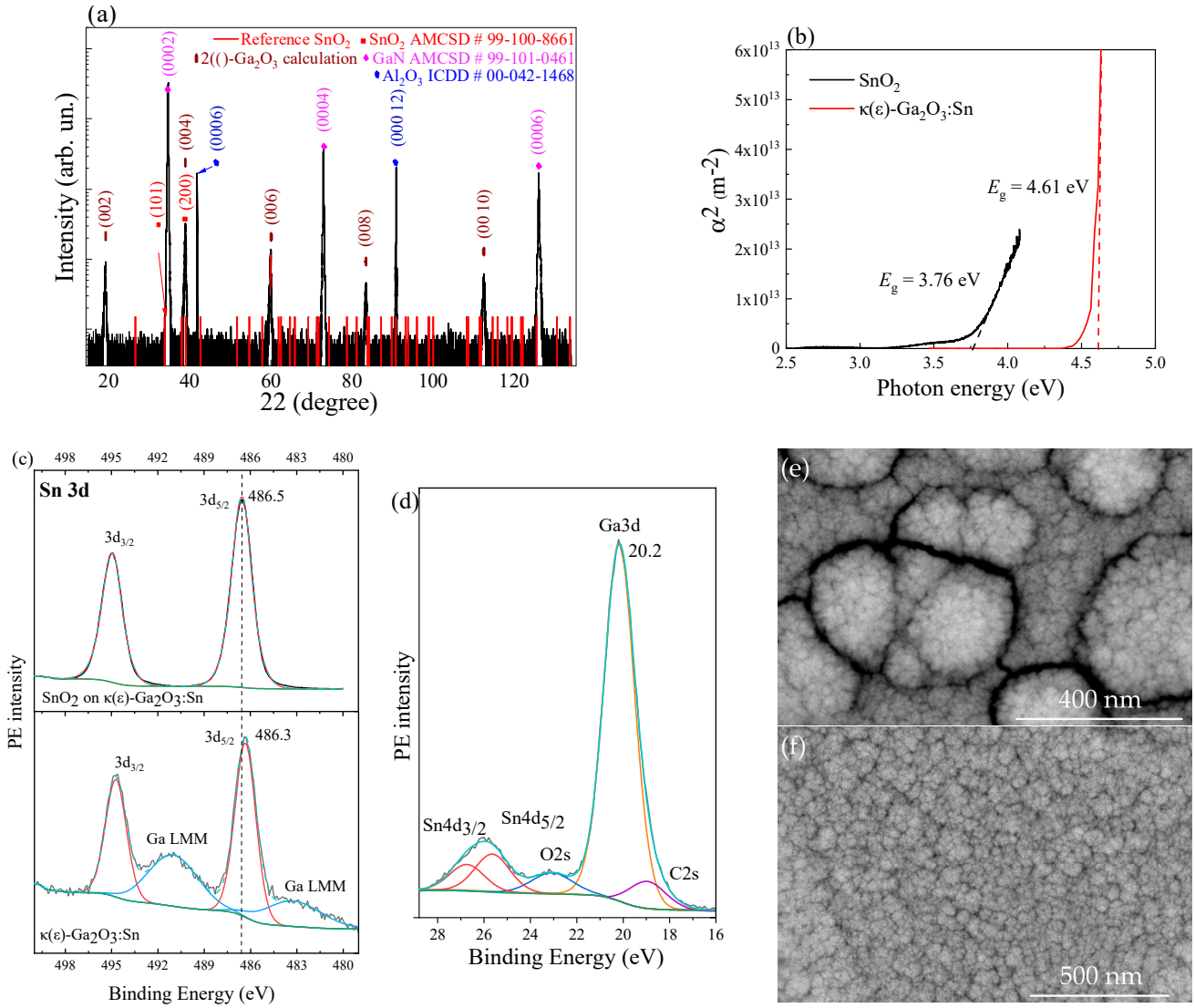

Figure 2. Structural characterization of the samples: (**a**) XRD pattern of the SnO_2/Ga_2O_3 heterostructure grown on GaN/Al_2O_3; (**b**) α^2 versus the photon energy for κ(ε)-Ga_2O_3:Sn and SnO_2 films; (**c**) Sn3d PE spectra of κ(ε)-Ga_2O_3:Sn and SnO_2 films; (**d**) Ga 3d, Sn 4d PE lines for κ(ε)-Ga_2O_3:Sn; FESEM images of the SnO_2 film deposited on Al_2O_3 (**e**) and κ(ε)-Ga_2O_3:Sn (**f**).

3.2. Gas-Sensitive Properties of the SnO_2/κ(ε)-Ga_2O_3:Sn heterostructure

The *I–V* characteristics of the SnO_2 thin films equipped with Pt contacts are linear in the range of applied voltages $U = -40$–40 V at *RT* as well as at higher *T*. Contrary to this, the *I–V* characteristics of the κ(ε)-Ga_2O_3:Sn films equipped with Pt contacts are nonlinear. The dependence of ln(*I*) on $U^{1/4}$ is linear, indicating the presence of a Schottky barrier at the Pt/κ(ε)-Ga_2O_3:Sn interface [24]. The I value through the Pt/κ(ε)-Ga_2O_3:Sn/Pt structures exceeds 0.1 A at $U > 12$ V which leads to the samples self-heating.

The SnO_2/κ(ε)-Ga_2O_3:Sn structure equipped with Pt contacts is a *n-N* isotype heterojunction and the Schottky barriers are connected in series. The *I–V* characteristics of such heterostructures are nonlinear and asymmetric as can be seen in Figure 3a. The $I(U = 4\text{ V})/I(U = -4\text{ V})$ ratio reaches the value of ~2×10^3 at $T = 25$ °C, then drops by half as *T* increases to 150 °C. The increase in reverse current with *T* rising is significantly higher than the increase in forward current. The forward-bias region of the *I–V* characteristics is approximated by the following function: $I_f = A_1 \times \exp(B_1 U)$, where I_f is a forward current; and A_1 and B_1 are the constants: $A_1 = (3.0 \pm 0.4) \times 10^{-6}$ A and $B_1 = 0.88 \pm 0.02$ V^{-1} at $T = 25$ °C. The reverse-bias region of the *I–V* characteristics can be approximated by a

similar function of $I_r = A_2 \times \exp(B_2 \mid U \mid)$, where I_r is a reverse current; A_2 and B_2 are the constants: $A_2 = (2.0 \pm 0.4) \times 10^{-9}$ A and $B_1 = 0.89 \pm 0.04$ V^{-1} at T = 25 °C. The forward-bias mode of the structure corresponds to the application of a positive potential to the SnO_2/Pt interface.

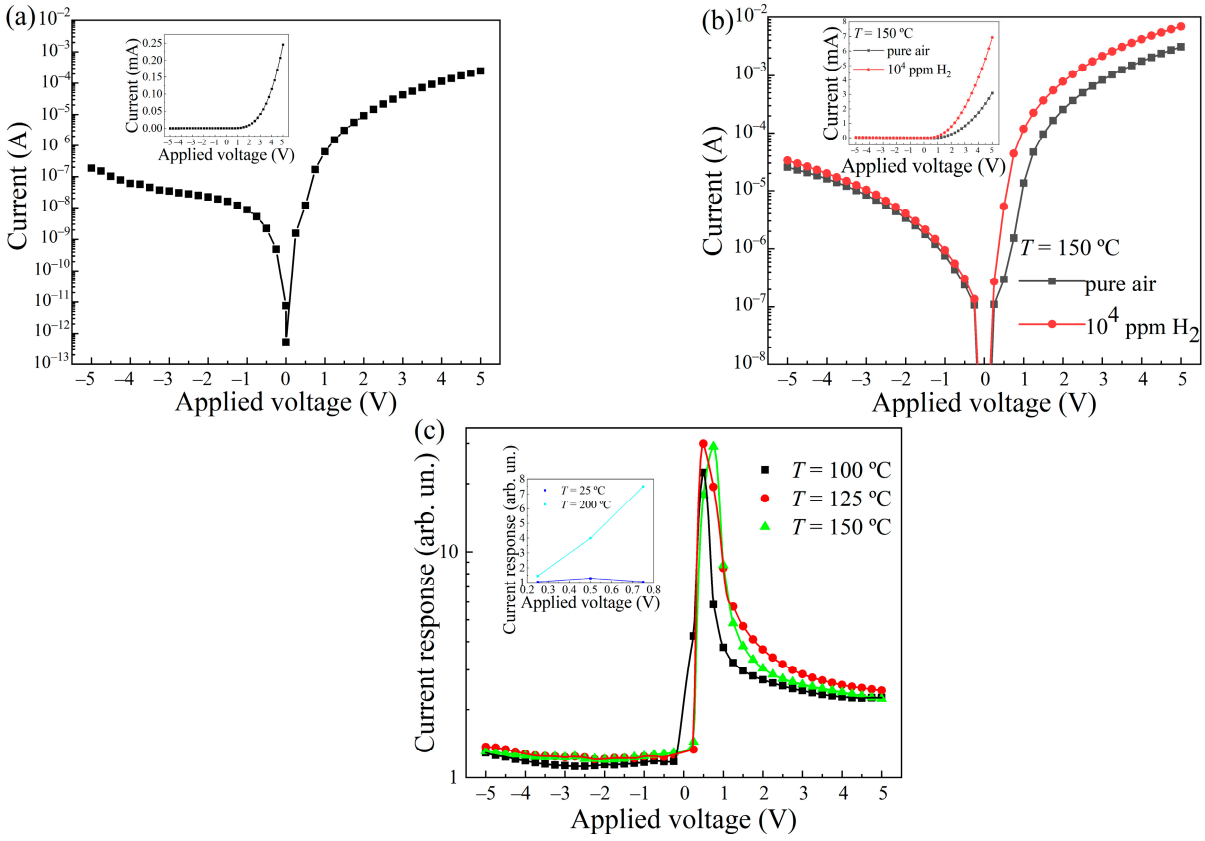

Figure 3. *I–V* characteristics of the SnO_2/κ(ε)-Ga_2O_3:Sn heterostructure at T = 25 °C in pure dry air in semi-logarithmic coordinates (**a**), at T = 150 °C under exposure to 10^4 ppm of H_2 (**b**). The insertions show these *I–V* characteristics in linear coordinates. Dependence of the response to 10^4 ppm H_2 on the applied voltage at different temperatures (**c**), the insertion shows the response to 10^4 ppm H_2 on the applied voltage at T = 25 °C and 200 °C.

Exposure to H_2 leads to a reversible increase in the I through heterostructures at T = 25–200 °C. Figure 3b shows the change in the *I–V* characteristics of the SnO_2/κ(ε)-Ga_2O_3:Sn heterostructure when exposed to 10^4 ppm of H_2 at T = 150 °C. The type of the functions, approximating the forward and reverse branches of the *I–V* characteristics, does not change with increasing T to 200 °C and under exposure to 10^4 ppm of H_2. The A_1 and A_2 increase, but B_1 and B_2 values decrease with T. The A_1 and A_2 values increase, whereas B_1 and B_2 practically do not change when exposed to H_2. Table 1 shows the A_1, A_2, B_1, and B_2 values at T = 150 °C and under exposure to 10^4 ppm of H_2.

Table 1. A_1, A_2, B_1, and B_2 at T = 150 °C and under exposure to 10^4 ppm H_2.

Conditions	A_1 (A)	A_2 (A)	B_1 (V^{-1})	B_2 (V^{-1})
Dry pure air	$(1.1 \pm 0.1) \times 10^{-4}$	$(1.1 \pm 0.1) \times 10^{-6}$	0.65 ± 0.03	0.65 ± 0.02
Dry pure air + 10^4 ppm H_2	$(2.6 \pm 0.3) \times 10^{-4}$	$(1.3 \pm 0.1) \times 10^{-6}$	0.66 ± 0.03	0.63 ± 0.03

To assess the effect of H_2 on the I through the $SnO_2/\kappa(\varepsilon)$-$Ga_2O_3$:Sn structures, the current response S_I was calculated based on the experimental I–V characteristics by the following ratio:

$$S_I = I_H / I_{air}, \quad (1)$$

where I_H is the current of the charge carrier through the $SnO_2/\kappa(\varepsilon)$-$Ga_2O_3$:Sn heterostructure in the gas mixture of pure dry air + H_2; I_{air} is the current of the charge carrier through the $SnO_2/\kappa(\varepsilon)$-$Ga_2O_3$:Sn heterostructure in pure dry air. The S_I values calculated on the basis of the experimental I–V characteristics and time dependences of currents at a fixed U (see Figure 4a) coincide. The S_I value depends on the magnitude and direction of the applied voltage (see Figure 3c). The highest response in the range of T = 100–125 °C was observed at U = 0.5 V, whereas the highest S_I was observed at U = 0.75 V at T = 150 °C. At room temperature, the maximum S_I was also noticed at U = 0.5 V (see Figure 3c, insertion). The response decreases exponentially with the applied voltage in the range of U = 1–5 V. S_I values are significantly lower at the reverse-bias mode and decrease slightly with an increase in the reverse voltage $|U_r|$ from 0.25 V to 2.5 V. Moreover, the response increases slightly with a further increase in $|U_r|$ to 5 V.

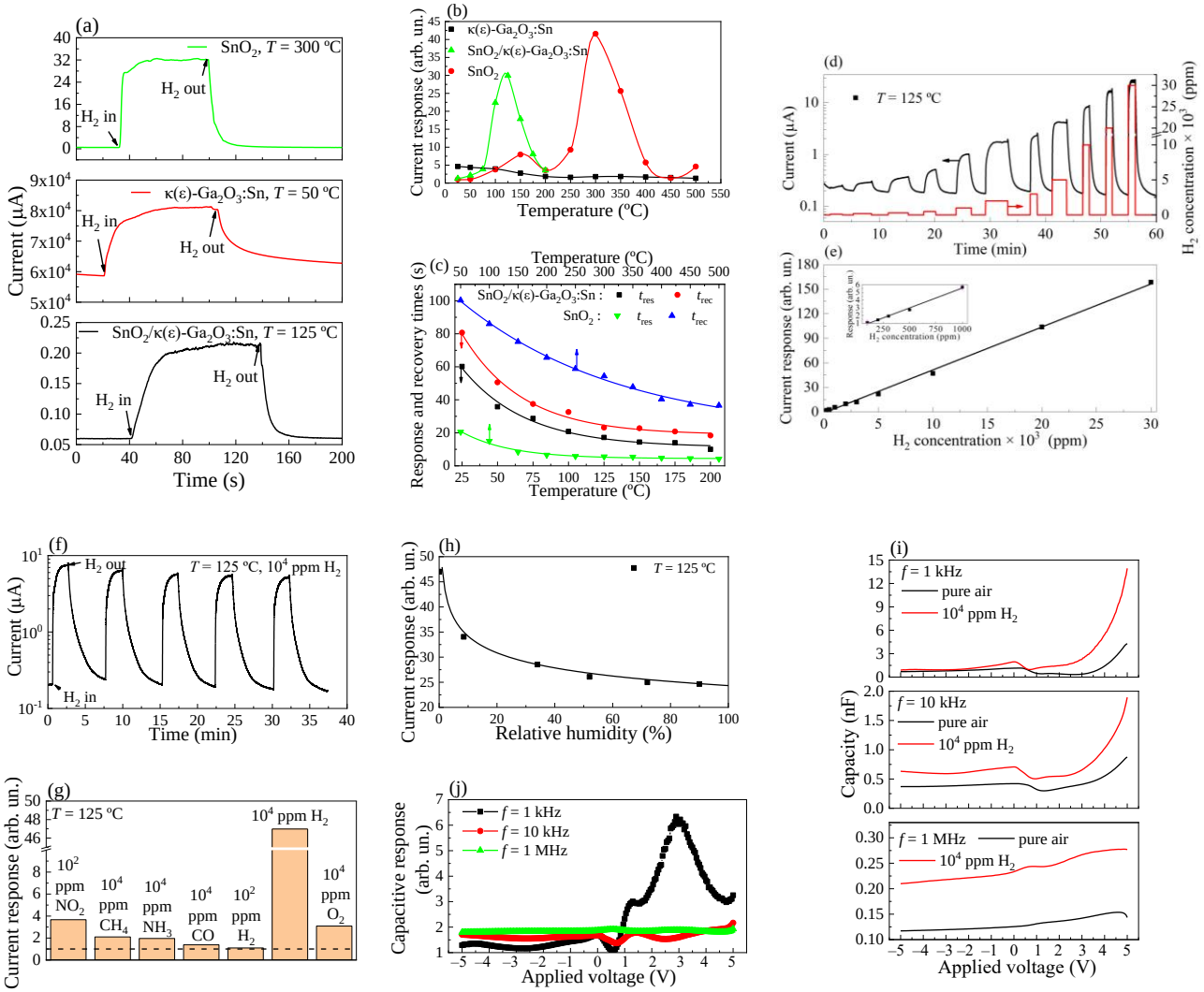

Figure 4. Gas-sensitive properties of *n-N* $SnO_2/\kappa(\varepsilon)$-$Ga_2O_3$:Sn heterostructure and other samples: (**a**) time dependences of current upon exposure to 10^4 ppm of H_2; (**b**) temperature dependences of

responses to 10^4 ppm of H_2; (**c**) temperature dependences of response and recovery times upon exposure to 10^4 ppm of H_2 for different samples; (**d**) time dependence of current upon exposure to different H_2 concentration; (**e**) dependence of response on H_2 concentration; (**f**) time dependence of current upon cyclic exposure to 10^4 ppm of H_2; (**g**) responses to fixed concentrations of NO_2, CH_4, NH_3, CO, H_2, and O_2; (**h**) effect of the relative humidity on responses to 10^4 ppm of H_2; (**i**) dependences of the capacitive response on applied voltage upon exposure to 10^4 ppm of H_2 at T = 125 °C and different frequencies; (**j**) effect of 10^4 ppm of H_2 on *C*-*V* characteristics at T = 125 °C and different frequencies; dependences in (**d**–**h**) were measured at T = 125 °C and U = 0.5 V.

The temperature dependences of the sample's response to 10^4 ppm of H_2 are presented in Figure 4b. The κ(ε)-Ga_2O_3:Sn films show the highest response to H_2 at T = 25 °C. The S_I of κ(ε)-Ga_2O_3:Sn films exceeds those of SnO_2 films in the temperature range of T = 25–50 °C; meanwhile, the S_I of κ(ε)-Ga_2O_3:Sn films decreases and S_I of SnO_2 films increases drastically with further increase in T. Sensitivity of SnO_2 and κ(ε)-Ga_2O_3:Sn films is based on reversible chemisorption of H_2 molecules on the semiconductor's surface according to the mechanisms described in refs. [14,25]. High sensitivity to H_2 at moderate temperatures (T = 300 °C) is characteristic of the SnO_2 thin films. Low S_I for the κ(ε)-Ga_2O_3:Sn films are caused by a significant influence of the bulk conductivity G_b, which does not depend on the charge state of the surface. The dependence of the SnO_2/κ(ε)-Ga_2O_3:Sn heterostructures response to H_2 on temperature is characterized by a maximum at T = 125 °C. These samples demonstrate the highest S_I in the range of T = 75–125 °C.

The experimental results displayed in Figure 4c prove that the SnO_2/κ(ε)-Ga_2O_3:Sn heterostructures are characterized by the high speed of operation compared to the SnO_2 thin films when exposed to H_2. The response t_{res} and recovery t_{rec} times were calculated to assess the speed of operation by the method described in ref. [9]. The calculated t_{res} and t_{rec} values can only be used to compare the speed of sensors operation at similar experimental conditions. t_{res} and t_{rec} decrease exponentially with T. t_{rec} and t_{res} + t_{rec} of the SnO_2/κ(ε)-Ga_2O_3:Sn structures are significantly lower than those of SnO_2 thin films at T = 25–200 °C. SnO_2 films are characterized by low t_{res}. The speed of operation for the κ(ε)-Ga_2O_3:Sn films was not evaluated due to their low responses at T > 50 °C. These samples are of interest for developing room temperature H_2 sensors. The t_{res} and t_{rec} of these films under exposure to 10^4 ppm of H_2 at T = 25 °C are 349.2 s and 379.6 s, respectively. Obviously, SnO_2/κ(ε)-Ga_2O_3:Sn heterostructures are the most interesting for highly sensitive H_2 sensors with high speed of operation and low operating temperatures. Therefore, our further attention will be focused on these structures.

The dependence of the SnO_2/κ(ε)-Ga_2O_3:Sn structure response on the H_2 concentration n_{H2} is linear (Figure 4d,e) in the n_{H2} range of 100–30000 ppm. The I_{air} and I_H of the SnO_2/κ(ε)-Ga_2O_3:Sn heterostructure decrease by 30% and 28%, respectively (see Figure 4f), during a cyclic exposure to H_2 (five cycles). At the same time, the current response decreased by only 17%. The observed decrease in response during cyclic exposure to H_2 is caused by the manifestation of chemisorbed hydrogen atoms with high binding energy. The temperature of 125 °C is not sufficient for the complete desorption of these hydrogen atoms from the semiconductor surface. Short-term heating of the structure at high temperatures can be used to regenerate the surface of semiconductors and for full desorption of H atoms [26]. The results of the long-term tests of the SnO_2/κ(ε)-Ga_2O_3:Sn heterostructures at T = 125 °C and when exposed to 10^4 ppm of H_2 demonstrated opposite changes of S_I. The samples after the experiments were stored in sealed packages. The long-term tests lasted 8 weeks with an interval between the experiments of 7–8 days. Just prior to each measurement the SnO_2/κ(ε)-Ga_2O_3:Sn heterostructures were subjected to heat at T = 500 °C for 90 s. There were increases in response from ~30 arb. un. to 47 arb. un. during the long-term tests. Response increases mostly due to a decrease in I_{air}. The most significant changes in response were in the first 4 weeks of testing.

The responses of the SnO_2/κ(ε)-Ga_2O_3:Sn heterostructure to NO_2, CH_4, NH_3, CO, and O_2 gases at T = 125 °C was measured to evaluate its selectivity (Figure 4g). Noteworthy, is that I through heterostructure increases reversibly when exposed to 10^4 ppm of CH_4,

NH_3h and CO. The response to these gases has been calculated by equation (1). The I_H was replaced by I_g, where I_g is the charge carrier current through the $SnO_2/\kappa(\varepsilon)$-$Ga_2O_3$:Sn heterostructure in the gas mixture of pure dry air + reducing gas (CH_4, NH_3, or CO). The responses to CH_4, NH_3, and CO are insignificant compared to the S_I to H_2, which equates to 29.92–46.98 arb. un. at T = 125 °C and $n_{H2} = 10^4$ ppm.

It was found, that the I value of the $SnO_2/\kappa(\varepsilon)$-$Ga_2O_3$:Sn reversibly decreases when exposed to NO_2 and O_2. The responses to NO_2 (S_{NO2}) and O_2 (S_{O2}) have been calculated by the following equations, correspondently:

$$S_{NO_2} = I_{air}/I_{NO_2}, \quad (2)$$

$$S_{O_2} = I_N/I_{O_2}, \quad (3)$$

where I_{NO_2} is the charge carrier current through the $SnO_2/\kappa(\varepsilon)$-$Ga_2O_3$:Sn heterostructure in the gas mixture of pure dry air + NO_2; I_N is the charge carrier current through the $SnO_2/\kappa(\varepsilon)$-$Ga_2O_3$:Sn heterostructure in the nitrogen atmosphere; I_{O_2} is the charge carrier current through the $SnO_2/\kappa(\varepsilon)$-$Ga_2O_3$:Sn heterostructure in the gas mixture of N_2 + O_2. S_I ratio when exposed to 100 ppm of H_2 at T = 125 °C happened to be 26.7 times lower than those for 100 ppm of NO_2 (Figure 4g). The $SnO_2/\kappa(\varepsilon)$-$Ga_2O_3$:Sn heterostructure also demonstrated relatively high response to O_2. The response to O_2 appears to be higher than to CH_4, NH_3, or CO at same concentration values. Hence, we have shown that $SnO_2/\kappa(\varepsilon)$-$Ga_2O_3$:Sn heterostructure is also attractive for developing highly sensitive NO_2 and O_2 sensors operating at low temperatures.

An increase in *RH* leads to a drop in the response of the $SnO_2/\kappa(\varepsilon)$-$Ga_2O_3$:Sn heterostructure to H_2 (Figure 4h). The most significant decrease in S_I occurs when *RH* increases from 0 to 34 %. In the range of *RH* = 34–90.0%, the response varies slightly.

Furthermore, the effect of 10^4 ppm of H_2 on the *C*-*V* characteristics of the $SnO_2/\kappa(\varepsilon)$-$Ga_2O_3$:Sn heterostructures at T = 125 °C and signal frequencies f = 1 kHz, 10 kHz, and 1 MHz have been studied. The results are illustrated in Figure 4i,j. Evidently, exposure to H_2 leads to a reversible increase in the electrical capacity of the structures. The capacitive response S_C has been calculated by the following equation:

$$S_C = C_H/C_{air}, \quad (4)$$

where C_H is the electrical capacitance of $SnO_2/\kappa(\varepsilon)$-$Ga_2O_3$:Sn heterostructure in the gas mixture of pure dry air + H_2; and C_{air} is the electrical capacitance of structures in pure dry air. Visibly, the S_C (see Figure 4i) is significantly lower than the S_I (Figure 3c). At f = 10 kHz and 1 MHz the capacitive response varies weakly. The highest S_C value is observed in the range of U = 0.95–5.00 V at f = 1 kHz and has a maximum at U = 2.9 V.

3.3. The Mechanism of the Sensory Effect

Initially, the resistance of the $Pt/\kappa(\varepsilon)$-Ga_2O_3:Sn interface is low and the Pt/SnO_2 contact is ohmic. The change in the potential barrier at $Pt/\kappa(\varepsilon)$-Ga_2O_3:Sn and Pt/SnO_2 interfaces upon exposure to gases can be neglected. The observed high responses of the $SnO_2/\kappa(\varepsilon)$-$Ga_2O_3$:Sn heterostructure at T = 25–175 °C; are due to the formation of the *n*-*N* isotypic heterojunction, where SnO_2 is the base.

Diffusion of H atoms up to the $SnO_2/\kappa(\varepsilon)$-$Ga_2O_3$:Sn interface at T = 25–175 °C; is unlikely. Changes of I and C upon exposure to H_2 occur mainly due to the chemisorption of gas molecules on semiconductor's surface. In the air atmosphere within a temperature range of T = 25–175 °C, the oxygen chemisorbs mainly in a molecular form on metal oxide semiconductors surface and captures electrons from their conduction band [25,27]. The reaction of reversible chemisorption of oxygen molecules can be represented as follows:

$$O_2 + S_a + e^- \leftrightarrow {O_2}^-_{(c)}, \quad (5)$$

where S_a is a free adsorption center; e is the electron charge; $O_2^-{}_{(c)}$ is the chemisorbed oxygen ion. As a result of reaction (4), an electron-depleted region is formed in the near-surface part of the semiconductor. A negative charge on the surface causes the upward of energy bands bending at eV_s, where V_s is the surface potential and $eV_s \sim N_i^2$, where N_i is the surface density of chemisorbed oxygen ions. In our case, the Debye length L_D for SnO_2 exceeds the grain size and the effect of grain boundaries on the transport of charge carriers in a semiconductor can be ignored. Oxygen chemisorption weakly changes the electrical conductivity of the κ(ε)-Ga_2O_3:Sn films due to the low contribution of the surface conductivity G_s to the total conductivity of G_t. Thus, changes in the current during the chemisorption of gases are mainly due to changes in the concentration of charge carriers in the SnO_2.

$G_t = G_b + G_s$ and the relationship between G_t and eV_s in our case is described by the following equation [28]:

$$G_t = G_b \times [1 - (L_D/D) \times [eV_s/(kT)]], \quad (6)$$

where D is the SnO_2 film thickness; k is the Boltzmann constant. An increase in the eV_s due to the oxygen molecule's chemisorption on the SnO_2 surface leads to a drop of G_t. The increase in G_t when exposed to H_2 is caused by the interaction of H_2 molecules with previously chemisorbed $O_2^-{}_{(c)}$ on the SnO_2 surface. This interaction can be represented as follows:

$$2H_2 + O_2^-{}_{(c)} \rightarrow 2H_2O + e^-. \quad (7)$$

As a result of reaction (7), a neutral H_2O molecule is formed and desorbed, an electron returns to the conduction band of SnO_2, the eV_s decreases and the finally G_t increases. When exposed to NO_2 the following reactions take place [29]:

$$\begin{gathered} NO_2 + S_a + e^- \rightarrow NO_2^-, \\ NO_2^- \rightarrow O^-{}_{(c)} + NO, \\ O^-{}_{(c)} + O^-{}_{(c)} \rightarrow O_2^-{}_{(c)} + e^- + S_a. \end{gathered} \quad (8)$$

NO_2 molecules chemisorb onto free adsorption centers and capture electrons from the SnO_2 conduction band. Meanwhile, eV_s is proportional to $(N_i + N_{NO2})^2$ in the mixtures of air + NO_2, where N_{NO2} is the surface density of chemisorbed NO_2^- ions [25,27]. An additional negative charge on the surface of the SnO_2 film leads to a greater decrease in G_t. Further, NO_2^- ions are dissociated to form chemisorbed $O^-{}_{(c)}$ ions and gaseous NO molecules. In the low temperature region, atomic $O^-{}_{(c)}$ ions associated to $O_2^-{}_{(c)}$ form and a free electron e^-, which returns to the conduction band of the semiconductor.

The κ(ε)-Ga_2O_3:Sn film is a source of electrons that are involved in reactions (5) and (8) with the gas molecules on the SnO_2 surface. This causes a high response of heterostructure at T = 75–175 °C. The base region (SnO_2) is filled with electrons from the κ(ε)-Ga_2O_3:Sn film with T rising, G_b of SnO_2 increases and the response decreases. SnO_2 films deposited on κ(ε)-Ga_2O_3:Sn are characterized by the absence of large agglomerates (see Figure 2e,f). This leads to an increase in the specific surface area of SnO_2 and the surface density of adsorption centers for gas molecules.

Table 2 shows a comparison of the responses and optimal operating temperatures of structures based on the Ga_2O_3 polymorphs when exposed to H_2 and NO_2 [9,14,18,19,30–42]. n_g is a gas concentration. SnO_2/κ(ε)-Ga_2O_3:Sn heterostructure in comparison with other items listed in this table is characterized by relatively high sensitivity to H_2 and NO_2 at a relatively low operating temperature. Ga2O3-based structures with higher responses to gases are characterized by high operating temperatures [9,30,34–37,41,42], low speed of operation [18,19], or are diode-type sensors based on high-cost materials [31,32,39]. SnO_2/κ(ε)-Ga_2O_3:Sn heterostructures demonstrate relatively high responses to H_2 and NO_2 at lower temperatures in comparison with the heterostructures based on other metal

oxides (see Table 3). Nano-structured heterostructures are characterized by higher responses to NO_2 but generally do not differ in high speed of operation.

Table 2. Gas-sensitive characteristics of structures based on Ga_2O_3 polymorphs.

Structure	n_g (ppm)	T (°C)	Response (arb. un.)	Ref.
		H_2		
α-Ga_2O_3:Sn	10^4	350	80	[9]
α-Ga_2O_3:Si	3×10^4	400	69.3	[30]
β-Ga_2O_3	500	*RT*	7.9×10^5	[31]
β-Ga_2O_3	2000	500	ΔI = 1.4 (mA)	[32]
β-Ga_2O_3	3×10^4	600	4	[33]
β-Ga_2O_3	200	300	6.3	[34]
β-Ga_2O_3:Cr_2O_3	2500	500	60	[35]
β-Ga_2O_3/Pd nanoclusters	10^4	625	~10^3	[36]
β-Ga_2O_3/SiO_2 (filter)	5000	700	~10^3	[37]
α-Ga_2O_3/κ(ϵ)-Ga_2O_3:Sn	2500	125	1.25	[38]
κ(ϵ)-Ga_2O_3	10^4	500	9.44	[14]
κ(ϵ)-Ga_2O_3:Sn	10^4	*RT*	1.2	
Pt/β-Ga_2O_3/GaN	1000	*RT*	229.8	[39]
β-Ga_2O_3/SnO_2	1000	400	8	[18]
β-Ga_2O_3/SnO_2	1000	200	7075.5	[19]
β-Ga_2O_3/WO_3	1000	200	4.1	[40]
SnO_2/κ(ε)-Ga_2O_3:Sn	1000	125	5.7	This work
	10^4		47	
		NO_2		
β-Ga_2O_3/ZnO	10	300	73.5	[41]
β-Ga_2O_3	200	800	5.1	[42]
β-Ga_2O_3/$La_{0.8}Sr_{0.2}CoO_3$			25.7	
SnO_2/κ(ε)-Ga_2O_3:Sn	100	125	3.7	This work

Table 3. Gas-sensitive characteristics of heterostructures based on different metal oxide semiconductors.

Structure	n_g (ppm)	T (°C)	Response (arb. un.)	Ref.
		H_2		
CeO_2/In_2O_3	50	160	20.7	[43]
SnO_2/ZnO	100	350	18.4	[44]
Pd/BN/ZnO	50	200	13	[45]
SnO_2/NiO	500	500	114	[46]
rGO/ZnO-SnO_2	100	380	9.4	[47]
RGO/ZnO	200	150	3.5	[48]
Al_2O_3/CuO	100	300	2.37	[49]
SnO_2/κ(ε)-Ga_2O_3:Sn	1000	125	5.7	This work
	10^4		47	
		NO_2		
m-WO_3/ZnO	1	150	167.8	[50]
WO_3/SnO_2	200	200	186	[51]
WO_3/MWCNT composite	5	150	18	[52]
ZnO/SWCNT composite	50	150	5	[53]
Sb_2O_3/In_2O_3 nanotubes	1	80	47	[54]
MoS_2/In_2O_3 nanotubes	50	RT	209	[55]
PdO/SnO_2 nanotubes	100	RT	20.3	[56]
TiO_2/ZnO nanotubes	5	RT	2.05	[57]
In_2O_3/ZnO	50	200	78	[58]
NiO/In_2O_3	10	145	532	[59]
SnO_2/κ(ε)-Ga_2O_3:Sn	100	125	3.7	This work

4. Conclusions

The structural and gas-sensitive properties of the *n-N* SnO_2/κ(ε)-Ga_2O_3:Sn heterostructures were investigated for the first time. The κ(ε)-Ga_2O_3:Sn and SnO_2 films were obtained by the halide vapor phase epitaxy and the high-frequency magnetron sputtering, respectively. The κ(ε)-Ga_2O_3:Sn crystalline film has a bandgap of 4.61 ± 0.01 eV. The SnO_2

nanocrystalline film has a bandgap of 3.76 ± 0.01 eV and is characterized by a developed microrelief of the surface, represented by grains with a size of ~35 nm. Exposure to H_2 leads to an increase in electrical current and capacitance of SnO_2/κ(ε)-Ga_2O_3:Sn structures. The current response of heterostructures to H_2 significantly exceeds the capacitive one. Gas sensor response and speed of operation of the SnO_2/κ(ε)-Ga_2O_3:Sn heterostructure under H_2 exposure overperform those of the single κ(ε)-Ga_2O_3:Sn and SnO_2 films in the temperature range of 25–175°C. This heterostructure demonstrates a low response to CO, NH_3, and CH_4 and a high response to NO_2 even at low concentrations. The current responses of SnO_2/κ(ε)-Ga_2O_3:Sn heterostructure to 10^4 ppm of H_2 and 100 ppm of NO_2 at 125 °C were 30–47 A.U. and 3.7 A.U., correspondingly. The sensory effect is realized mainly due to the chemisorption of gas molecules on the SnO_2 surface, which is the base region of the heterostructure. The κ(ε)-Ga_2O_3:Sn film is a source of electrons that are involved in reactions with gas molecules on the SnO_2 film surface. The SnO_2 film deposited on the κ(ε)-Ga_2O_3:Sn film is characterized by a more developed surface microstructure. This leads to an increase in the surface density of adsorption centers for gas molecules. The advantages of the SnO_2/κ(ε)-Ga_2O_3:Sn heterostructure for gas sensors are shown, the main one being high sensitivity at relatively low operating temperatures. Doubtfully, this structure has every chance of being the base of the sensor.

Author Contributions: Conceptualization, A.A. and V.N.; methodology, V.K., P.B., P.K., J.D., A.P., A.K. and E.Z; software, V.K., P.B., P.K., J.D., A.P., A.K. and E.Z.; validation, A.A. and V.N.; formal analysis, A.A., N.Y., V.K., P.B., P.K., J.D., A.P., A.K. and E.Z.; investigation, N.Y., V.K., J.D., A.P., A.K. and E.Z.; resources, A.A., V.N., J.D., A.P., A.K. and E.Z.; data curation, A.A., N.Y., P.B., A.P., A.K. and E.Z; writing—original draft preparation, A.A., V.N., P.B. and P.K.; writing—review and editing, A.A., N.Y., V.N., P.B., P.K. and J.D.; visualization, A.A., N.Y., P.B., P.K., A.P., A.K. and E.Z.; supervision, A.A. and V.N.; project administration, A.A.; funding acquisition, A.A. All authors have read and agreed to the published version of the manuscript.

Funding: This research was funded by the Russian Science Foundation, grant number 20-79-10043. Viktor Kopyev acknowledges the support of the grant under the Decree of the Government of the Russian Federation No. 220 of 9 April 2010 (Agreement No. 075-15-2022-1132 of 1 July 2022).

Institutional Review Board Statement: Not applicable.

Informed Consent Statement: Not applicable.

Data Availability Statement: All data that support the findings of this study are included within the article.

Acknowledgments: The FESEM investigations have been carried out using the equipment of Share Use Centre "Nanotech" of the ISPMS SB RAS. XPS studies were carried out using the equipment of the resource center "Physical Methods of Surface Investigation" (Saint Petersburg University Research Park). We are grateful to Bogdan Kushnarev from Research and Development Centre for Advanced Technologies in Microelectronics at National Research Tomsk State University for the deposition of tin oxide and platinum films.

Conflicts of Interest: The authors declare no conflict of interest.

References

1. Das, S.; Jayaraman, V. SnO_2: A comprehensive review on structures and gas sensors. *Prog. Mater. Sci.* **2014**, *66*, 112–255. [CrossRef]
2. Zhu, J.; Xu, Z.; Ha, S.; Li, D.; Zhang, K.; Zhang, H.; Feng, J. Gallium Oxide for Gas Sensor Applications: A Comprehensive Review. *Materials* **2022**, *15*, 7339. [CrossRef] [PubMed]
3. Zhai, H.; Wu, Z.; Fang, Z. Recent progress of Ga_2O_3-based gas sensors. *Ceram. Int.* **2022**, *48*, 24213–24233. [CrossRef]
4. Gogova, D.; Suwardi, A.; Kuznetsova, Y.; Zatsepin, A.; Mochalov, L.; Nezhdanov, A.; Szyszka, B. Lanthanum-doped barium stannate-a new type of critical raw materials-free transparent conducting oxide. *J. Adv. Appl. Phys. Res.* **2017**, *4*, 1–8. [CrossRef]
5. Jeon, H.M.; Leedy, K.D.; Look, D.C.; Chang, C.S.; Muller, D.A.; Badescu, S.C.; Vasilyev, V.; Brown, J.L.; Green, A.J.; Chabak, K.D. Homoepitaxial β-Ga_2O_3 transparent conducting oxide with conductivity σ = 2323 S cm^{-1}. *Appl. Mater.* **2021**, *9*, 101105. [CrossRef]

6. Dalapati, G.; Sharma, H.; Guchhait, A.; Chakrabarty, N.; Bamola, P.; Liu, Q.; Saianand, G.; Ambati, M.; Mukhopadhyay, S.; Dey, A.; et al. Tin oxide for optoelectronic, photovoltaic and energy storage devices: A review. *J. Mater. Chem. A* **2021**, *9*, 16621–16684. [CrossRef]
7. Yang, S.; Lei, G.; Xu, H.; Lan, Z.; Wang, Z.; Gu, H. Metal Oxide Based Heterojunctions for Gas Sensors: A Review. *Nanomaterials* **2021**, *11*, 1026. [CrossRef]
8. Mahmoud, W.E. Solar blind avalanche photodetector based on the cation exchange growth of β-Ga_2O_3/SnO_2 bilayer heterostructure thin film. *Sol. Energy Mater. Sol. Cells* **2016**, *152*, 65–72. [CrossRef]
9. Almaev, A.; Nikolaev, V.; Yakovlev, N.; Butenko, P.; Stepanov, S.; Pechnikov, A.; Scheglov, M.; Chernikov, E. Hydrogen sensors based on Pt/α-Ga_2O_3:Sn/Pt structures. *Sens. Actuators B Chem.* **2022**, *364*, 131904. [CrossRef]
10. Smirnov, A.P.N.; Shchemerov, I.; Yakimov, E.; Pearton, S.; Ren, F.; Chernykh, A.; Gogova, D.; Kochkova, A. Electrical Properties, Deep Trap and Luminescence Spectra in Semi-Insulating, Czochralski β-Ga_2O_3 (Mg). *ECS J. Solid State Sci. Technol.* **2019**, *8*, Q3019. [CrossRef]
11. Gogova, D.; Ghezellou, M.; Tran, D.; Richter, S.; Papamichail, A.; Hassan, J.; Persson, A.; Persson, P.; Kordina, O.; Monemar, B.; et al. Epitaxial growth of β-Ga_2O_3 by hot-wall MOCVD. *AIP Adv.* **2022**, *12*, 055022. [CrossRef]
12. Yakimov, E.; Polyakov, A.; Nikolaev, V.; Pechnikov, A.; Scheglov, M.; Yakimov, E.; Pearton, S. Electrical and Recombination Properties of Polar Orthorhombic κ-Ga_2O_3 Films Prepared by Halide Vapor Phase Epitaxy. *Nanomaterials* **2023**, *13*, 1214. [CrossRef] [PubMed]
13. Biswas, M.; Nishinaka, H. Thermodynamically metastable α-, ε- (or κ-), and γ-Ga_2O_3: From material growth to device applications. *APL Mater.* **2022**, *10*, 060701. [CrossRef]
14. Almaev, A.; Nikolaev, V.; Butenko, P.; Stepanov, S.; Pechnikov, A.; Yakovlev, N.; Sinyugin, I.; Shapenkov, S.; Scheglov, M. Gas sensors based on pseudohexagonal phase of gallium oxide. *Phys. Status Solidi B* **2021**, *259*, 2100306. [CrossRef]
15. Nikolaev, V.; Stepanov, S.; Pechnikov, A.; Shapenkov, S.; Scheglov, M.; Chikiryaka, A.; Vyvenko, O. HVPE Growth and Characterization of ε-Ga_2O_3 Films on Various Substrates. *ECS J. Solid State Sci. Technol.* **2020**, *9*, 45014. [CrossRef]
16. Parisini, A.; Mazzolini, P.; Bierwagen, O.; Borelli, C.; Egbo, K.; Sacchi, A.; Bosi, M.; Seravalli, L.; Tahraoui, A.; Fornari, R. Study of SnO/ϵ-Ga_2O_3 p–n diodes in planar geometry. *J. Vac. Sci.* **2022**, *40*, 42701. [CrossRef]
17. Budde, M.; Splith, D.; Mazzolini, P.; Tahraoui, A.; Feldl, J.; Ramsteiner, M.; Wenckstern, H.; Grundmann, M.; Bierwagen, O. SnO/β-Ga_2O_3 vertical pn heterojunction diodes. *Appl. Phys. Lett.* **2020**, *117*, 252106. [CrossRef]
18. Jang, Y.; Kim, W.; Kim, D.; Hong, S. Fabrication of Ga_2O_3/SnO_2 core–shell nanowires and their ethanol gas sensing properties. *J. Mater. Res.* **2011**, *26*, 2322–2327. [CrossRef]
19. Abdullah, Q.; Ahmed, A.; Ali, A.; Yam, F.; Hassan, Z.; Bououdina, M. Novel SnO_2-coated β-Ga_2O_3 nanostructures for room temperature hydrogen gas sensor. *Int. J. Hydrogen Energy* **2021**, *46*, 7000–7010. [CrossRef]
20. Boiko, M.; Sharkov, M.; Boiko, A.; Konnikov, S.; Bobyl, A.; Budkina, N. Investigation of the Atomic, Crystal, and Domain Structures of Materials Based on X-Ray Diffraction and Absorption Data: A Review. *Technic. Phys.* **2015**, *60*, 1575–1600. [CrossRef]
21. Maksimova, N.; Sevastyanov, E.; Chernikov, E.; Korusenko, P.; Nesov, S.; Kim, S.; Biryukov, A.; Sergeychenko, N.; Davletkildeev, N.; Sokolov, D. Sensors based on tin dioxide thin films for the detection of pre-explosive hydrogen concentrations. *Sens. Actuators B Chem.* **2021**, *341*, 130020. [CrossRef]
22. Maksimova, N.; Almaev, A.; Sevastyanov, E.; Potekaev, A.; Chernikov, E.; Sergeychenko, N.; Korusenko, P.; Nesov, S. Effect of Additives Ag and Rare-Earth Elements Y and Sc on the Properties of Hydrogen Sensors Based on Thin SnO_2 Films during Long-Term Testing. *Coatings* **2019**, *9*, 423. [CrossRef]
23. Mahmoodinezhad, A.; Janowitz, C.; Naumann, F.; Plate, P.; Gargouri, H.; Henkel, K.; Schmeißer, D.; Flege, J. Low-temperature growth of gallium oxide thin films by plasma-enhanced atomic layer deposition. *J. Vac. Sci. Technol. A* **2020**, *38*, 022404. [CrossRef]
24. Elhadidy, H.; Sikula, J.; Franc, J. Symmetrical current–voltage characteristic of a metal–semiconductor–metal structure of Schottky contacts and parameter retrieval of a CdTe structure. *Semicond. Sci. Technol.* **2012**, *27*, 15006. [CrossRef]
25. Gaman, V. Basic physics of semiconductor hydrogen sensors. *Russ. Phys. J.* **2008**, *51*, 425. [CrossRef]
26. Korotcenkov, G.; Cho, B. Instability of metal oxide-based conductometric gas sensors and approaches to stability improvement (short survey). *Sens. Actuators B* **2011**, *156*, 527–538. [CrossRef]
27. Afzal, A. β-Ga_2O_3 nanowires and thin films for metal oxide semiconductor gas sensors: Sensing mechanisms and performance enhancement strategies. *J. Mater.* **2019**, *5*, 542–557. [CrossRef]
28. Simion, C.; Schipani, F.; Papadogianni, A.; Stanoiu, A.; Budde, M.; Oprea, A.; Weimar, U.; Bierwagen, O.; Barsan, N. Conductance Model for Single-Crystalline/Compact Metal Oxide Gas-Sensing Layers in the Nondegenerate Limit: Example of Epitaxial SnO_2(101). *ACS Sens.* **2019**, *4*, 2420–2428. [CrossRef]
29. Badalyan, S.; Rumyantseva, M.; Smirnov, V.; Alikhanyan, A.; Gaskov, A. Effect of Au and NiO catalysts on the NO_2 sensing properties of nanocrystalline SnO_2. *Inorg. Mater.* **2010**, *46*, 232–236. [CrossRef]
30. Yakovlev, N.; Almaev, A.; Butenko, P.; Tetelbaum, D.; Mikhaylov, A.; Nikolskaya, A.; Pechnikov, A.; Stepanov, S.; Boiko, M.; Chikiryaka, À.; et al. Effect of Si^+ Ion Implantation in α-Ga_2O_3 Films on Their Gas Sensitivity. *IEEE Sens. J.* **2022**, *23*, 1885–1895. [CrossRef]
31. Jang, S.; Jung, S.; Kim, J.; Ren, F.; Pearton, S.J.; Baik, K.H. Hydrogen Sensing Characteristics of Pt Schottky Diodes on (−201) and (010) Ga_2O_3 Single Crystals. *ECS J. Solid State Sci. Technol.* **2018**, *7*, Q3180. [CrossRef]

32. Nakagomi, S.; Yokoyama, K.; Kokubun, Y. Devices based on series-connected Schottky junctions and β-Ga_2O_3/SiC heterojunctions characterized as hydrogen sensors. *J. Sens. Sens. Syst.* **2014**, *3*, 231–239. [CrossRef]
33. Fleischer, M.; Giber, J.; Meixner, H. H_2-induced changes in electrical conductance of β-Ga_2O_3 thin-film systems. *Appl. Phys. A.* **1992**, *54*, 560–566. [CrossRef]
34. Cuong, N.D.; Park, Y.W.; Yoon, S.G. Microstructural and electrical properties of Ga_2O_3 nanowires grown at various temperatures by vapor–liquid–solid technique. *Sens. Actuators B.* **2009**, *140*, 240–244. [CrossRef]
35. Almaev, A.; Chernikov, E.; Novikov, V.; Kushnarev, B.; Yakovlev, N.; Chuprakova, E.; Oleinik, V.; Lozinskaya, A.; Gogova, D. Impact of Cr_2O_3 additives on the gas-sensitive properties of β-Ga_2O_3 thin films to oxygen, hydrogen, carbon monoxide, and toluene vapors. *J. Vac. Sci. Technol. A* **2021**, *39*, 23405. [CrossRef]
36. Bausewein, A.; Hacker, B.; Fleischer, M.; Meixner, H. Effects of Palladium Dispersions on Gas-Sensitive Conductivity of Semiconducting Ga_2O_3 Thin-Film Ceramics. *J. Am. Ceram. Soc.* **1997**, *80*, 317–323. [CrossRef]
37. Fleischer, M.; Kornely, S.; Weh, T.; Frank, J.; Meixner, H. Selective gas detection with high-temperature operated metal oxides using catalytic filters. *Sens. Actuators B.* **2000**, *69*, 205–210. [CrossRef]
38. Almaev, A.; Nikolaev, V.; Stepanov, S.; Pechnikov, A.; Chikiryaka, A.; Yakovlev, N.; Kalygina, V.; Kopyev, V.; Chernikov, E. Hydrogen influence on electrical properties of Pt-contacted α-Ga_2O_3/ε-Ga_2O_3 structures grown on patterned sapphire substrates. *J. Phys. D Appl. Phys.* **2020**, *53*, 414004. [CrossRef]
39. Yan, J.; Lee, C. Improved detection sensitivity of Pt/β-Ga_2O_3/GaN hydrogen sensor diode. *Sens. Actuators B.* **2009**, *143*, 192–197. [CrossRef]
40. Park, S.; Kim, S.; Sun, G.-J.; Lee, C. Synthesis, structure and ethanol sensing properties of Ga_2O_3-core/WO_3-shell nanostructures. *Thin Solid Films.* **2015**, *591*, 341–345. [CrossRef]
41. Jin, C.; Park, S.; Kim, H.; Lee, C. Ultrasensitive multiple networked Ga_2O_3-core/ZnO-shell nanorod gas sensors. *Sens. Actuators B* **2012**, *161*, 223–228. [CrossRef]
42. Zhang, B.; Lin, H.; Gao, H.; Lu, X.; Nam, C.; Gao, P. Perovskite-sensitized β-Ga_2O_3 nanorod arrays for highly selective and sensitive NO_2 detection at high temperature. *J. Mater. Chem. A* **2020**, *8*, 10845–10854. [CrossRef]
43. Hu, J.; Sun, Y.J.; Xue, Y.; Zhang, M.; Li, P.W.; Lian, K.; Zhuiykov, S.; Zhang, W.D.; Chen, Y. Highly sensitive and ultra-fast gas sensor based on CeO_2-loaded In_2O_3 hollow spheres for ppb-level hydrogen detection. *Sens. Actuators B* **2018**, *257*, 124–135. [CrossRef]
44. Park, S.; Ko, H.; Kim, S.; Lee, C. Role of the interfaces in multiple networked one-dimensional core-shell nanostructured gas sensors. *ACS Appl. Mater. Interfaces* **2014**, *6*, 9595–9600. [CrossRef] [PubMed]
45. Weber, M.J.; Kim, Y.; Lee, J.; Kim, J.; Iatsunskyi, I.; Coy, E.; Miele, P.; Bechelany, M.; Kim, S. Highly efficient hydrogen sensors based on Pd nanoparticles supported on boron nitride coated ZnO nanowires. *J. Mater. Chem. A* **2019**, *7*, 8107–8116. [CrossRef]
46. Raza, M.; Kaur, N.; Pinna, E.C.N. Toward optimized radial modulation of the space-charge region in one-dimensional SnO_2–NiO core-shell nanowires for hydrogen sensing. *ACS Appl. Mater. Interfaces* **2020**, *12*, 4594–4606. [CrossRef]
47. Zhang, X.; Sun, J.; Tang, K.; Wang, H.; Chen, T.; Jiang, K.; Zhou, T.; Quan, H.; Guo, R. Ultralow detection limit and ultrafast response/recovery of the H_2 gas sensor based on Pd-doped rGO/ZnO-SnO_2 from hydrothermal synthesis. *Microsyst. Nanoeng.* **2022**, *8*, 67. [CrossRef]
48. Anand, K.; Singh, O.; Singh, M.; Kaur, J.; Singh, R. Hydrogen sensor based on graphene/ZnO nanocomposite. *Sens. Actuators B* **2014**, *195*, 409–415. [CrossRef]
49. Lupan, O.; Ababii, N.; Mishra, A.K.; Bodduluri, M.T.; Magariu, N.; Vahl, A.; Krüger, H.; Wagner, B.; Faupel, F.; Adelung, R.; et al. Heterostructure-based devices with enhanced humidity stability for H_2 gas sensing applications in breath tests and portable batteries. *Sens. Actuators A* **2021**, *329*, 112804. [CrossRef]
50. Sun, J.; Sun, L.; Han, N.; Pan, J.; Liu, W.; Bai, S.; Feng, Y.; Luo, R.; Li, D.; Chen, A. Ordered mesoporous WO_3/ZnO nanocomposites with isotype heterojunctions for sensitive detection of NO_2. *Sens. Actuators B* **2019**, *285*, 68–75. [CrossRef]
51. Bai, S.; Li, D.; Han, D.; Luo, R.; Chen, A.; Chung, C. Preparation, characterization of WO_3–SnO_2 nanocomposites and their sensing properties for NO_2. *Sens. Actuators B* **2010**, *150*, 749–755. [CrossRef]
52. Hung, N.; Chinh, N.; Nguyen, T.; Kim, E.; Choi, G.; Kim, C.; Kim, D. Carbon nanotube-metal oxide nanocomposite gas sensing mechanism assessed via NO_2 adsorption on n-WO_3/p-MWCNT nanocomposites. *Ceram. Int.* **2020**, *46*, 29233–29243. [CrossRef]
53. Barthwal, S.; Singh, B.; Singh, N.B. ZnO-SWCNT nanocomposite as NO_2 gas sensor. *Mater. Today Proc.* **2018**, *5*, 15439–15444. [CrossRef]
54. Du, W.; Wu, L.; Zhao, J.; Si, W.; Wang, F.; Liu, J.; Liu, W. Engineering the surface structure of porous indium oxide hexagonal nanotubes with antimony trioxide for highly-efficient nitrogen dioxide detection at low temperature. *Appl. Surf. Sci.* **2019**, *484*, 853–863. [CrossRef]
55. Yang, Z.; Zhang, D.; Chen, H. MOF-derived indium oxide hollow microtubes/MoS_2 nanoparticles for NO_2 gas sensing. *Sens. Actuators B* **2019**, *300*, 127037. [CrossRef]
56. Teng, L.; Liu, Y.; Ikram, M.; Liu, Z.; Ullah, M.; Ma, L.; Zhang, X.; Wu, H.; Li, L.; Shi, K. One-step synthesis of palladium oxide-functionalized tin dioxide nanotubes: Characterization and high nitrogen dioxide gas sensing performance at room temperature. *J. Colloid Interface Sci.* **2019**, *537*, 79–90. [CrossRef] [PubMed]
57. Choi, H.; Kwon, S.; Lee, W.; Im, K.; Kim, T.; Noh, B.; Park, S.; Oh, S.; Kim, K. Ultraviolet Photoactivated Room Temperature NO_2 Gas Sensor of ZnO Hemitubes and Nanotubes Covered with TiO_2 Nanoparticles. *Nanomaterials* **2020**, *10*, 462. [CrossRef]

58. Zhao, C.; Bai, J.; Gong, H.; Liu, S.; Wang, F. Tailorable morphology of core-shell nanofibers with surface wrinkles for enhanced gas-sensing properties. *ACS Appl. Nano Mater.* **2018**, *1*, 6357–6367. [CrossRef]
59. Xie, J.; Liu, X.; Jing, S.; Pang, C.; Liu, Q.; Zhang, J. Chemical and electronic modulation via atomic layer deposition of NiO on porous In_2O_3 films to boost NO_2 detection. *ACS Appl. Mater. Interfaces* **2021**, *13*, 39621–39632. [CrossRef]